$\delta(^{17}O)$ of the aqueous HCl (37%) for **4**: $\delta = 27.5$;[22] of the aqueous NaOH for **4a**: $\delta = 5.3$; $\Delta\nu_{1/2}$ in each case 55 Hz. $\delta(^1H)$ of the HCl (37%) for **4**: $\delta = 7.00$; of the aqueous NaOH at **4a**: $\delta = 3.77$. Spectra simulations: Bruker WIN-DAISY, version 4.0. Deconvolution: Bruker WIN1D-NMR, version 6.0. Measurement temperature: **4** 300 K; **4a** 358 K; **4a** deuterated in $D_2O$ 365 K. Isotope shifts: $^1\Delta^{31}P_A(^{13}C^X) = -0.009$ relative to [per-$^{12}$C]-isotopomer; $^{13}CH_2/^{13}CHD$ $^1\Delta^{13}C(^2H) = -0.38$; $CH_2/CHD$ $^1\Delta^1H(^2H) = -0.020$ [from $^1H\{^{31}P\}$ spectra].[20, 23]

[12] E. Fluck, G. Heckmann, R. Janoschek, E. Gorbunowa, M. Westerhausen, unpublished results.
[13] R. C. Hirst, D. M. Grant, E. G. Paul, *J. Chem. Phys.* **1966**, *44*, 4305 – 4315.
[14] Z. S. Novikova, A. A. Prishchenko, I. F. Lutsenko, *J. Gen. Chem. USSR* **1977**, 2409 – 2410; *Zh. Obshch. Khim*. **1977**, *47*, 2636 – 2637.
[15] L. Maier, *Helv. Chim. Acta* **1970**, *53*, 1948 – 1956.
[16] M. M. Crutchfield, C. F. Callis, R. R. Irani, G. C. Roth, *Inorg. Chem.* **1962**, *1*, 813 – 817.
[17] D. B. Trowbridge, G. L. Kenyon, *J. Am. Chem. Soc.* **1970**, *92*, 2181 – 2182.
[18] D. B. Trowbridge, D. M. Yamamoto, G. L. Kenyon, *J. Am. Chem. Soc.* **1972**, *94*, 3816 – 3824.
[19] G. Heckmann, E. Fluck, *Rev. Heteroat. Chem.* **1994**, *11*, 65 – 87.
[20] G. Heckmann, F. Rosche, F. Weller, E. Fluck, *Phosphorus Sulfur Silicon* **1996**, *115*, 3 – 18.
[21] J. A. Gerlt, P. C. Demou, S. Mehdi, *J. Am. Chem. Soc.* **1982**, *104*, 2848 – 2856.
[22] I. P. Gerothanassis, J. Lauterwein, *Magn. Reson. Chem.* **1986**, *24*, 1034 – 1038.
[23] P. E. Hansen, *Prog. Nucl. Magn. Reson. Chem.* **1988**, *20*, 207 – 255.
[24] L. C. Thomas, R. A. Chittenden, *Spectrochim. Acta* **1970**, *26a*, 781 – 800.

# Evolving Opportunities in Structure Solution from Powder Diffraction Data—Crystal Structure Determination of a Molecular System with Twelve Variable Torsion Angles**

Benson M. Kariuki, Patrizia Calcagno, Kenneth D. M. Harris,* Douglas Philp,* and Roy L. Johnston*

In general, determination of crystal structures from single-crystal diffraction data can be carried out in a routine and straightforward manner. However, many crystalline solids can be obtained only as microcrystalline powders and are not suitable for investigation by single-crystal diffraction methods. In the past, this problem has limited the ability to determine the structural properties of such materials. There is clearly a pressing need to develop and exploit techniques for solving crystal structures from *powder* diffraction data.[1–3] However, although traditional techniques for structure solution from powder diffraction data have been applied successfully in several cases, these techniques have certain intrinsic limitations,[2] and organic molecular crystals represent a particularly challenging case. For these reasons, our recent research has focused on the development and implementation of new methodologies for structure solution from powder diffraction data, and has led to new "direct-space" approaches for structure solution which overcome some of these difficulties. Such direct-space techniques are particularly suited to the case of molecular crystal structures. Herein, we demonstrate the current state-of-the-art in the solution of molecular crystal structures from powder diffraction. To our knowledge, the structure reported here is the most complex molecular crystal structure, solved directly from powder diffraction data, that has so far been reported in the literature.

Direct-space approaches[2, 4, 5] for structure solution from powder diffraction data are based on sampling trial crystal structures in direct space. Structural models are generated independently of the powder diffraction data, with the "quality" of each structural model assessed by comparison between the powder diffraction pattern calculated for the structural model and the experimental powder diffraction pattern. In our work, this comparison is based on the profile $R$ factor $R_{wp}$,[6] as used in Rietveld refinement. We emphasize that $R_{wp}$ considers the whole digitized intensity profile, and thus uses the raw powder diffraction data directly "as measured". Peak overlap is implicitly taken care of, and the need to extract integrated intensities $I(hkl)$ for individual reflections from the powder diffraction pattern is circumvented. In effect, our direct-space approach searches the $R_{wp}(\mathbf{X})$ hypersurface to find the best structure solution (lowest $R_{wp}$), where $\{\mathbf{X}\}$ represents the set of variables that define the structure. In direct-space strategies for structure solution, the structure is defined by a "structural fragment", which represents an appropriate collection of atoms within the asymmetric unit. The variables in $\{\mathbf{X}\}$ represent the position, orientation, and intramolecular geometry of the structural fragment. The position is specified by the coordinates $\{x, y, z\}$ of the center of mass or a predefined pivot atom, the orientation is specified by rotation angles $\{\theta, \phi, \psi\}$ around a set of orthogonal axes, and the intramolecular geometry is specified by a set of variable torsion angles $\{\tau_1, \tau_2, \ldots, \tau_n\}$. In general, the bond lengths, bond angles, and any known torsion angles (i.e. if aspects of the molecular conformation are known a priori) are fixed in the structure solution calculation, and are taken either from standard values for the type of molecule under study or from the known geometry of a similar molecule. Previous research has demonstrated the success of Monte Carlo,[4, 7–13] simulated annealing,[5, 14–16] and genetic algorithm[17–22] methods for searching $R$ factor hypersurfaces to locate the global minimum (structure solution). Most of these direct-space approaches have considered hypersurfaces based on the profile $R$ factor $R_{wp}$ (as in this paper), although hypersurfaces based on other definitions of agreement factor have also been considered.[16, 20–22] In all of these methods for global optimization, the main limitation is the number of variables in $\{\mathbf{X}\}$ (the number of degrees of freedom which define the hypersurface) and early applications of direct-space approaches for structure solution focused on examples of essentially rigid molecules, with at most a few variable torsion angles. The generalization of direct-space

[*] Prof. K. D. M. Harris, Dr. D. Philp, Dr. R. L. Johnston, Dr. B. M. Kariuki, P. Calcagno
School of Chemistry, University of Birmingham
Edgbaston, Birmingham B15 2TT (UK)
Fax: (+44) 121-414-7473
E-mail: k.d.m.harris@bham.ac.uk

[**] We are grateful to EPSRC and the University of Birmingham for financial support.

  1433-7851/99/3806-0831 $ 17.50+.50/0 

approaches for structure solution of molecular crystals from powder diffraction data requires that structures of complex systems, defined by a significant number of torsional degrees of freedom, can be solved in a straightforward and reliable manner.

Here we report the application of our genetic algorithm approach to solve the crystal structure of heptamethylene-1,7-bis(diphenylphosphane oxide) $Ph_2P(O)(CH_2)_7P(O)Ph_2$ (Figure 1) from powder diffraction data. This compound is of importance within our systematic studies[23, 24] of crystal packing and crystal engineering of phosphane oxides and their co-crystals.

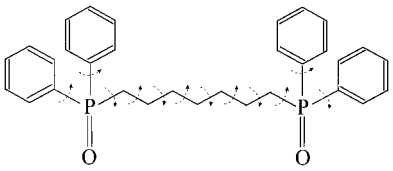


Figure 1. The structural formula of $Ph_2P(O)(CH_2)_7P(O)Ph_2$, showing the variable torsion angles considered in the genetic algorithm structure solution calculation.

In our genetic algorithm approach for structure solution (Scheme 1), a population of trial crystal structures is allowed to evolve subject to the normal rules and operations that govern evolutionary systems. Full details of our methodology are given in reference [19]. Initially, the population comprises a set of random structures (total number $N_P$). For the case with one molecule in the asymmetric unit, a given structure is specified by the position $\{x, y, z\}$, orientation $\{\theta, \phi, \psi\}$, and intramolecular geometry $\{\tau_1, \tau_2, \tau_3, \ldots, \tau_n\}$ of the structural fragment, and these variables represent the "genetic code" that uniquely characterizes each member of the population. The profile $R$ factor $R_{wp}$ is taken to indicate the quality ("fitness") of each structure in the population, where a low $R_{wp}$ value (good agreement between experimental and calculated powder diffraction data) corresponds to high fitness and a high $R_{wp}$ value corresponds to low fitness. It is advantageous to define a fitness function, and several different fitness functions have been considered in our work.[19] In the present case, the linear fitness function $F(\rho) = 1 - \rho$ was used, where $\rho = (R_{wp} - R_{min})/(R_{max} - R_{min})$ and $R_{min}$ and $R_{max}$ represent the minimum and maximum values of $R_{wp}$ in the current population (the values of $R_{min}$ and $R_{max}$ are updated as the population evolves under the genetic algorithm). The use of $\rho$ in the definition of the fitness function introduces the advantages of dynamic scaling. The population is allowed to evolve through a number of (typically a few hundred) generations (Scheme 1), using the operations of mating, mutation, and natural selection. In the *mating* procedure, a given number ($N_M$) of pairs of structures ("parents") are selected from the population, with the probability of selecting a given structure proportional to its fitness. New structures ("offspring") are then generated by combining genetic information from the two parents. Thus, mating does not introduce any new genetic material into the population but redistributes the existing genetic material. The *mutation* procedure, on the other hand, introduces new genetic material into the population. In each generation, a given number ($N_X$) of structures are selected at random from the current population and random changes are made to parts of their genetic code to create mutant structures. Note that the original structures from which the mutants are derived are retained within the population. The introduction of mutants is important to ensure that genetic diversity is maintained throughout the evolution of the population. The *natural selection* procedure ensures that only the best structures survive from one generation to the next, which leads to a continual improvement in the overall quality of the population. After the population has evolved for a sufficiently large number of generations, the fittest member of the population (the structure with lowest $R_{wp}$) should, in principle, be close to the correct crystal structure.

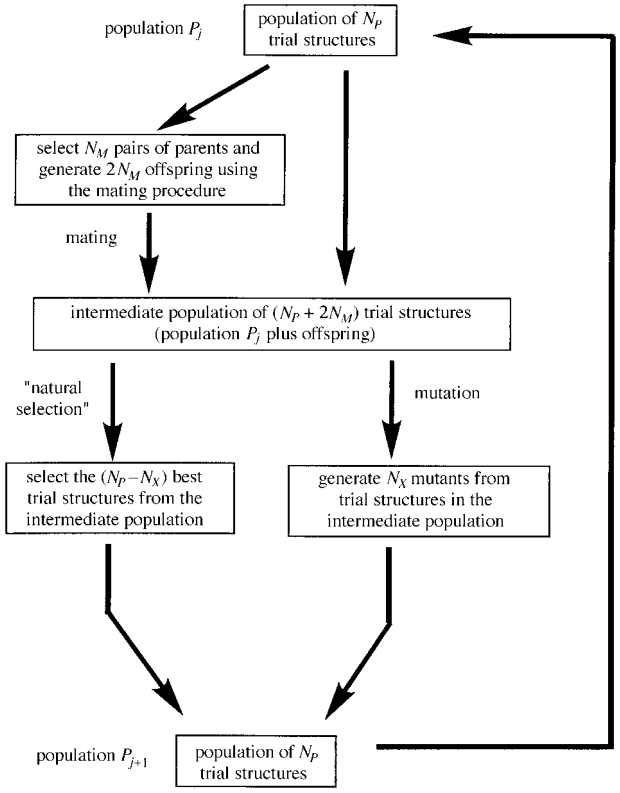


Scheme 1. Flow chart representing the evolution of the population from one generation (population $P_j$) to the next generation (population $P_{j+1}$) in our genetic algorithm approach for structure solution.

The powder X-ray diffraction pattern of $Ph_2P(O)(CH_2)_7P(O)Ph_2$ was recorded using a conventional laboratory powder X-ray diffractometer,[25] and the unit cell and space group were determined directly from the powder diffraction pattern.[26]

In the genetic algorithm structure solution calculation, the structural fragment comprised all non-hydrogen atoms of the molecule. Standard bond lengths and bond angles were used,[24, 28] and the atoms of each benzene ring and all atoms directly bonded to it were constrained to be planar. The molecule was subjected to translation and rotation within the unit cell, together with variation of all twelve torsion angles (Figure 1) that define the molecular conformation. Thus, each structure considered in the genetic algorithm calculation was defined by eighteen variables $\{x, y, z, \theta, \phi, \psi, \tau_1, \tau_2, \tau_3, \ldots, \tau_{12}\}$.

  1433-7851/99/3806-0832 $ 17.50+.50/0 

The genetic algorithm structure solution calculation was carried out using the program GAPSS,[19, 29] and involved the evolution of 500 generations of a population of 100 structures ($N_P$). In each generation, 100 offspring ($N_M = 50$) and 20 mutations ($N_X$) were considered. For the mating and mutation procedures, the eighteen variables were considered in terms of fourteen groups $\{x, y, z\}$, $\{\theta, \phi, \psi\}$, $\{\tau_1\}$, $\{\tau_2\}$, $\{\tau_3\}$, ..., $\{\tau_{12}\}$. In carrying out a given mating operation between two parents, the fourteen groups from each parent were distributed between the two offspring, with no restriction on which combination of groups may come from each parent (in each mating operation, this was determined on a random basis). In carrying out the mutation procedure on a selected structure, seven groups were selected at random, and a new random value was assigned to one variable within each of the selected groups (thus, when the group {x, y, z} or the group $\{\theta, \phi, \psi\}$ is selected, only one of the three variables was changed). The evolution of $R_{wp}$ during the genetic algorithm structure solution calculation is shown in Figure 2, and demonstrates clearly that the overall quality of the population improves as the population evolves. The lowest value of $R_{wp}$ in the population decreases significantly, with evidence for the occurrence of a particularly significant evolutionary event at generation 163.

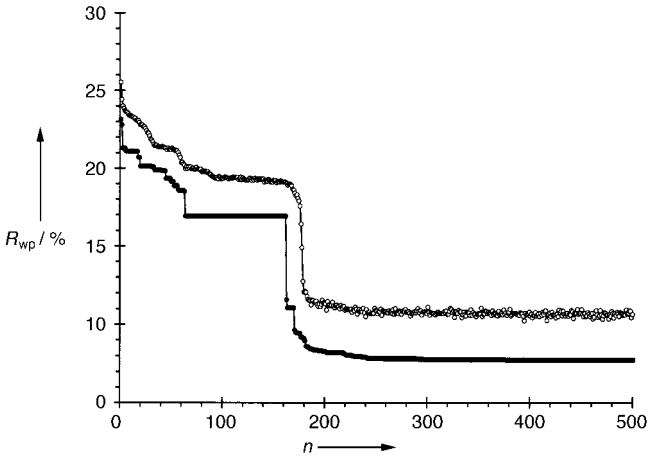


Figure 2. Evolutionary progress plot showing the evolution of $R_{wp}$ for the best structure in the population (filled circles) and the average $R_{wp}$ for the structures in the population (open circles) as a function of generation number ($n$) in the genetic algorithm calculation.

The best structure (the structure with lowest $R_{wp}$ in the final generation) was taken as the starting structural model for Rietveld refinement using the GSAS program package.[30] The positions of all non-hydrogen atoms were refined, with standard geometric restraints applied to the bond lengths and bond angles. A common isotropic displacement parameter was fixed at $U_{iso} = 0.025$ Å$^2$ for all atoms. In the final stages, a preferred orientation parameter was refined. The final Rietveld refinement (Figure 3) gave $R_{wp} = 0.050$ and $R_p = 0.038$. Details of the final refined structure are given in Table 1.

The successful structure solution of $Ph_2P(O)(CH_2)_7P(O)Ph_2$ reported here using experimental data collected on a conventional laboratory powder X-ray diffractometer emphasizes

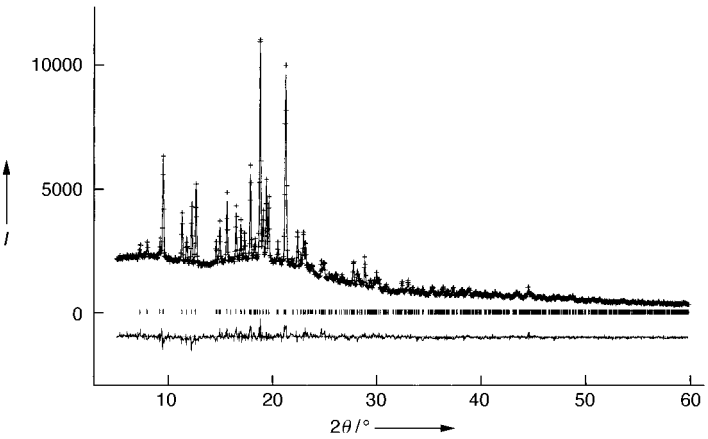


Figure 3. Experimental (+ marks), calculated (solid line) and difference (lower line) powder X-ray diffraction profiles for the Rietveld refinement of $Ph_2P(O)(CH_2)_7P(O)Ph_2$. Reflection positions are marked. The calculated powder diffraction profile is for the final refined crystal structure, details of which are given in Table 1.

Table 1. Fractional coordinates for the non-hydrogen atoms in the final refined crystal structure of $Ph_2P(O)(CH_2)_7P(O)Ph_2$ ($P2_1/n$; $a = 12.560(1)$, $b = 10.203(1)$, $c = 22.889(2)$ Å, $\beta = 105.53(1)^\circ$).

| Atom | x/a | y/b | z/c |
|---|---|---|---|
| C(1) | 0.224(2) | 0.940(2) | 0.6306(5) |
| C(2) | 0.299(3) | 0.989(4) | 0.6830(6) |
| C(3) | 0.290(3) | 0.953(4) | 0.7404(5) |
| C(4) | 0.209(3) | 0.862(4) | 0.7457(7) |
| C(5) | 0.137(3) | 0.809(4) | 0.694(1) |
| C(6) | 0.146(3) | 0.845(3) | 0.6361(7) |
| C(7) | 0.205(1) | 1.173(1) | 0.558(1) |
| C(8) | 0.097(1) | 1.223(1) | 0.549(2) |
| C(9) | 0.080(2) | 1.356(2) | 0.557(2) |
| C(10) | 0.171(2) | 1.442(1) | 0.573(3) |
| C(11) | 0.277(2) | 1.394(1) | 0.577(2) |
| C(12) | 0.294(1) | 1.261(1) | 0.570(2) |
| P(1) | 0.227(1) | 0.998(1) | 0.5565(6) |
| O(1) | 0.144(2) | 0.932(2) | 0.5067(6) |
| C(13) | 0.366(2) | 0.977(1) | 0.553(1) |
| C(14) | 0.413(2) | 0.844(2) | 0.573(1) |
| C(15) | 0.486(2) | 0.790(2) | 0.536(1) |
| C(16) | 0.509(3) | 0.645(2) | 0.5459(7) |
| C(17) | 0.562(5) | 0.610(2) | 0.611(1) |
| C(18) | 0.568(5) | 0.464(2) | 0.623(1) |
| C(19) | 0.612(3) | 0.418(1) | 0.687(1) |
| P(2) | 0.628(1) | 0.245(1) | 0.6950(5) |
| O(2) | 0.542(1) | 0.170(2) | 0.6507(7) |
| C(20) | 0.766(1) | 0.209(3) | 0.6889(7) |
| C(21) | 0.782(2) | 0.164(4) | 0.634(1) |
| C(22) | 0.889(2) | 0.147(5) | 0.628(1) |
| C(23) | 0.980(1) | 0.168(5) | 0.677(1) |
| C(24) | 0.965(1) | 0.208(5) | 0.733(1) |
| C(25) | 0.858(1) | 0.226(5) | 0.739(1) |
| C(26) | 0.631(2) | 0.207(1) | 0.7726(6) |
| C(27) | 0.663(4) | 0.303(2) | 0.8179(6) |
| C(28) | 0.668(4) | 0.273(2) | 0.8782(6) |
| C(29) | 0.635(4) | 0.149(2) | 0.8929(7) |
| C(30) | 0.597(4) | 0.055(2) | 0.847(1) |
| C(31) | 0.596(5) | 0.084(2) | 0.787(1) |

that, in order to achieve successful structure solution from powder diffraction data, it is not essential that synchrotron X-ray powder diffraction data are used. This fact has also been demonstrated by several previous examples (see reference [2] for a more detailed discussion).

  1433-7851/99/3806-0833 $ 17.50+.50/0 

In the crystal structure of $Ph_2P(O)(CH_2)_7P(O)Ph_2$ (Figure 4 top), the molecule adopts an unexpected (but completely rational) conformation (Figure 4 bottom), with one *gauche* bond in the $(CH_2)_7$ chain and the other parts of the chain close to all-*trans* conformations. It could not have been predicted in advance that this specific conformation would be adopted in the crystal structure, which emphasizes the importance of allowing complete conformational flexibility in the structure solution calculation. In this conformation, the two P=O groups in a given molecule are brought into an almost parallel alignment, and the $P(O)Ph_2$ end-groups of neighboring molecules interact through a series of C–H···O and C–H···π interactions. This structure exhibits very interesting contrasts to the structures of other members of the homologous family $Ph_2P(O)(CH_2)_nP(O)Ph_2$. A full description and rationalization of the crystal structure of $Ph_2P(O)(CH_2)_7P(O)Ph_2$, and comparison with others in the $Ph_2P(O)(CH_2)_n(O)Ph_2$ family, will be given in a future paper.[24]

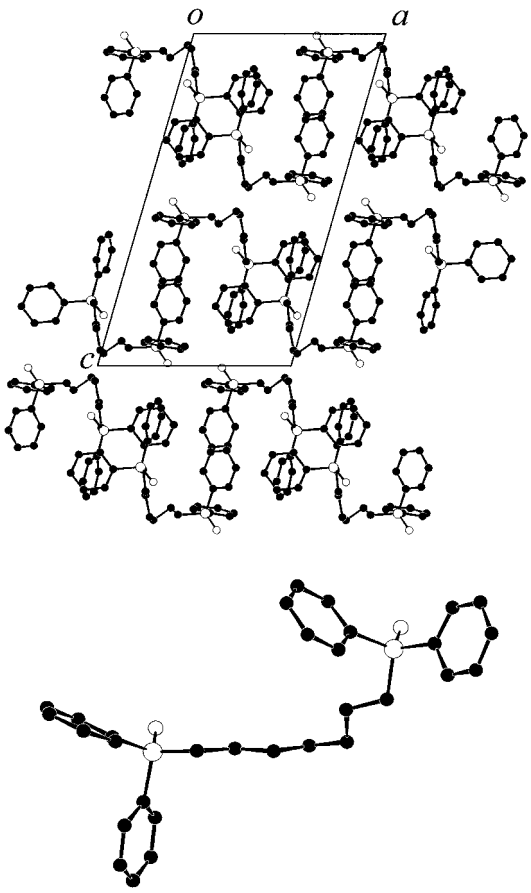


Figure 4. Top: Final refined crystal structure of $Ph_2P(O)(CH_2)_7P(O)Ph_2$ (hydrogen atoms not shown) viewed along the *b* axis. Bottom: Conformation of the $Ph_2P(O)(CH_2)_7P(O)Ph_2$ molecule in the crystal structure.

The successful determination of a molecular crystal structure defined by eighteen structural degrees of freedom demonstrates clearly the increasing scope and potential of techniques for the solution of molecular crystal structures from powder diffraction data. Indeed, the opportunities demonstrated here augur well for future successful applications of our techniques to solve molecular crystal structures of even greater complexity.

Received: October 6, 1998 [Z12498IE]
German version: *Angew. Chem.* **1999**, *111*, 860–864

**Keywords:** genetic algorithm technique · phosphanes · structure elucidation · X-ray powder diffraction

[1] A. K. Cheetham, A. P. Wilkinson, *Angew. Chem.* **1992**, *104*, 1594; *Angew. Chem. Int. Ed. Engl.* **1992**, *31*, 1557.
[2] K. D. M. Harris, M. Tremayne, *Chem. Mater.* **1996**, *8*, 2554.
[3] D. M. Poojary, A. Clearfield, *Acc. Chem. Res.* **1997**, *30*, 414.
[4] K. D. M. Harris, M. Tremayne, P. Lightfoot, P. G. Bruce, *J. Am. Chem. Soc.* **1994**, *116*, 3543.
[5] J. M. Newsam, M. W. Deem, C. M. Freeman, *NIST Spec. Publ.* **1992**, *846*, 80 (*Accuracy in Powder Diffraction II*).
[6] The definition of $R_{wp}$ is given in Equation (1) where $y_i$(obs) is the intensity of the *i*th data point in the experimental powder diffraction

$$R_{wp} = 100 \times \left( \frac{\sum_i w_i (y_i(\text{obs}) - y_i(\text{calcd}))^2}{\sum_i w_i (y_i(\text{obs}))^2} \right)^{1/2} \quad (1)$$

profile, $y_i$(calcd) is the intensity of the *i*th data point in the calculated powder diffraction profile, and $w_i$ is a weighting factor for the *i*th data point. Thus, $R_{wp}$ considers the whole digitized intensity profile, as measured, rather than the integrated intensities of individual diffraction maxima.
[7] B. M. Kariuki, D. M. S. Zin, M. Tremayne, K. D. M. Harris, *Chem. Mater.* **1996**, *8*, 565.
[8] D. Ramprasad, G. P. Pez, B. H. Toby, T. J. Markley, R. M. Pearlstein, *J. Am. Chem. Soc.* **1995**, *117*, 10694.
[9] M. Tremayne, B. M. Kariuki, K. D. M. Harris, *J. Appl. Crystallogr.* **1996**, *29*, 211.
[10] M. Tremayne, B. M. Kariuki, K. D. M. Harris, *J. Mater. Chem.* **1996**, *6*, 1601.
[11] M. Tremayne, B. M. Kariuki, K. D. M. Harris, *Angew. Chem.* **1997**, *109*, 788; *Angew. Chem. Int. Ed. Engl.* **1997**, *36*, 770.
[12] M. Tremayne, B. M. Kariuki, K. D. M. Harris, K. Shankland, K. S. Knight, *J. Appl. Crystallogr.* **1997**, *30*, 968.
[13] L. Elizabé, B. M. Kariuki, K. D. M. Harris, M. Tremayne, M. Epple, J. M. Thomas, *J. Phys. Chem. B* **1997**, *101*, 8827.
[14] Y. G. Andreev, P. Lightfoot, P. G. Bruce, *Chem. Commun.* **1996**, 2169.
[15] Y. G. Andreev, G. S. MacGlashan, P. G. Bruce, *Phys. Rev. B* **1997**, *55*, 12011.
[16] W. I. F. David, K. Shankland, N. Shankland, *Chem. Commun.* **1998**, 931.
[17] B. M. Kariuki, H. Serrano-González, R. L. Johnston, K. D. M. Harris, *Chem. Phys. Lett.* **1997**, *280*, 189.
[18] K. D. M. Harris, R. L. Johnston, B. M. Kariuki, M. Tremayne, *J. Chem. Res.* **1998**, 390.
[19] K. D. M. Harris, R. L. Johnston, B. M. Kariuki, *Acta Crystallogr. Sect. A* **1998**, *54*, 632.
[20] K. Shankland, W. I. F. David, T. Csoka, *Z. Kristallogr.* **1997**, *212*, 550.
[21] K. Shankland, W. I. F. David, T. Csoka, L. McBride, *Int. J. Pharm.* **1998**, *165*, 117.
[22] T. Csoka, W. I. F. David, K. Shankland, *Mater. Sci. Forum* **1998**, *278–281*, 294.
[23] B. M. Kariuki, K. D. M. Harris, D. Philp, J. M. A. Robinson, *J. Am. Chem. Soc.* **1997**, *119*, 12679.
[24] P. Calcagno, B. M. Kariuki, S. J. Kitchin, J. M. A. Robinson, D. Philp, K. D. M. Harris, unpublished results.
[25] The powder X-ray diffraction pattern of $Ph_2P(O)(CH_2)_7P(O)Ph_2$ was recorded at 22 °C in transmission mode on a Siemens D5000 diffractometer, with Ge-monochromated $Cu_{K\alpha 1}$ radiation and a linear position-sensitive detector covering 8° in 2$\theta$. The total range of 2$\theta$ was 5° to 60°, measured in 0.02° steps and collected over 6 h.

  1433-7851/99/3806-0834 $ 17.50+.50/0 

[26] The powder X-ray diffraction pattern was indexed (using the first 20 observable peaks) by the program ITO,[27] to give the unit cell: $a=12.59$, $b=10.20$, $c=22.89$ Å, $\beta=105.5^\circ$. Systematic absences are consistent with the monoclinic space group $P2_1/n$. Density considerations suggest that there is one molecule in the asymmetric unit.
[27] J. W. Visser, *J. Appl. Crystallogr.* **1969**, *2*, 89.
[28] F. H. Allen, O. Kennard, D. G. Watson, L. Brammer, A. G. Orpen, R. Taylor, *J. Chem. Soc. Perkin Trans. 2*, **1987**, S1.
[29] R. L. Johnston, B. M. Kariuki, K. D. M. Harris, *GAPSS*, Genetic Algorithm for Powder Structure Solution, University of Birmingham, **1997**.
[30] A. C. Larson, R. B. Von Dreele, Los Alamos Lab. Report No. LA-UR-86-748, **1987**.

## Preparation and Properties of Nanoporous Triblock Copolymer Membranes**

Guojun Liu,* Jianfu Ding, and Sean Stewart

A block copolymer is a linear macromolecule consisting of different monomers in long sequences. $(A)_n(B)_m(C)_l$, for example, denotes a triblock consisting of $n$ units of monomer A, $m$ units of B, and $l$ units of C in sequence. The different blocks of most block copolymers are incompatible. They segregate in bulk, and each block forms domains with a specific shape. At block segregation equilibrium, the domain shape of a given block in a diblock copolymer, the simplest type of block copolymer, is determined by the composition of the diblock, and the domain shape/composition relation is well understood.[1] The morphologies of triblocks are, however, far more complex and less well understood because they are determined by two independent composition variables, the sequence of block linkage and the interfacial tensions between the different blocks. The domain shape of the minor component, which exists in the least amount in a triblock, ranges from spheres[2, 3] to cylinders,[3–9] dumbbells,[10] and layers.[2, 3, 6] The cylinders can be straight[3–6] or folded into loops[6, 7] or spirals.[7] The cylinders can also be tortuous and interconnected.[8, 9] The domain size of the minor component can be tuned by varying the molar mass of the block and has a very narrow distribution. The domains can be regularly packed. Because of these properties, films of block copolymers are ideal precursors for membranes with nanometer-sized channels or nanochannels. The nanochannels can be produced by full[11, 12] or partial decomposition[13, 14] of the cylindrical domains formed from one of the blocks, as was demonstrated for diblock films.[11–14]

[*] Prof. G. Liu, Dr. J. Ding, S. Stewart
Department of Chemistry, University of Calgary
2500 University Drive, NW, Calgary, AB, T2N 1N4 (Canada)
Fax: (+1) 403-289-9488
E-mail: gliu@acs.ucalgary.ca

[**] This research was supported by the Petroleum Research Fund, administered by the American Chemical Society (G.L. and J.D.), the Natural Sciences and Engineering Research Council of Canada (S.S.), and the University of Calgary (S.S.).

Here we report the first preparation of thin films with nanochannels from a triblock copolymer, polyisoprene-*block*-poly(2-cinnamoylethyl methacrylate)-*block*-poly(*tert*-butyl acrylate) or PI-*b*-PCEMA-*b*-P*t*BA **1**. The polymer consists of $3.7\times10^2$ units of isoprene, $4.2\times10^2$ units of CEMA, and

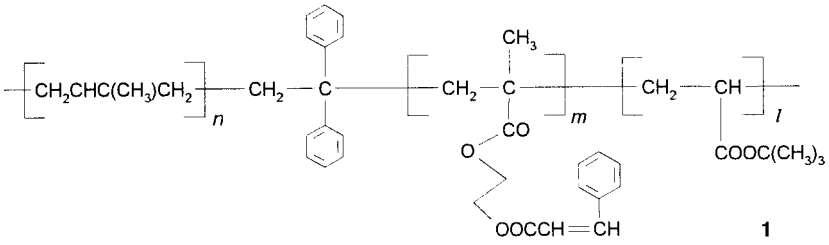


**1**

$5.5\times10^2$ units of *t*BA. Ten weight portions of this triblock were mixed with one portion of a homopolymer P*t*BA (HP*t*BA) with approximately $1.0\times10^2$ units of *t*BA. At this mixing ratio, the P*t*BA block of the triblock and HP*t*BA form a seemingly novel continuous phase in the matrix of PI-*b*-PCEMA (Scheme 1). The PCEMA block was crosslinked by

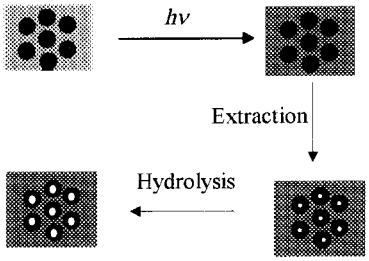


Scheme 1. Strategy for the preparation of nanoporous membranes. P*t*BA/HP*t*BA domains (black circles) do not form hexagonally packed cylinders in the system studied, and the cross-sectional view of hexagonally packed cylinders is shown here for convenience in drawing only. UV irradiation crosslinks the PCEMA domains in the PI-*b*-PCEMA matrix (gray rectangle). Extraction of HP*t*BA out of the P*t*BA/HP*t*BA domains yields membranes with nanochannels (white dots). Larger nanochannels (white circles) are produced by both extracting HP*t*BA and removing the *tert*-butyl groups in the P*t*BA block.

UV photolysis. Instead of generating nanochannels by the traditional block degradation method, we prepared membranes more conveniently in this study by extracting HP*t*BA out of the cast films with methylene chloride. Such extracted films had gas-permeability constants roughly 6 orders of magnitude higher than that of low-density polyethylene films. Membranes with even greater gas permeability were obtained by both extracting HP*t*BA and also removing the *tert*-butyl groups from the P*t*BA block by hydrolysis (see Scheme 1).

The polymer PI-*b*-P(TMS-HEMA)-*b*-P*t*BA (TMS = trimethylsilyl, HEMA = 2-hydroxyethyl methacrylate), the precursor to triblock **1**, was synthesized by combining procedures we used for the synthesis of PI-*b*-P(TMS-HEMA)[15, 16] and P(TMS-HEMA)-*b*-P*t*BA.[13, 14, 17] The exact reactions are outlined in Scheme 2. Isoprene polymerization was carried out in dry hexane at room temperature for two days with *sec*-butyllithium as the initiator. The other two blocks were

  1433-7851/99/3806-0835 $ 17.50+.50/0 